Renewable Energy 99 (2016) 898–910

Contents lists available at ScienceDirect

Renewable Energy

journal homepage: www.elsevier.com/locate/renene

Turbulent kinetic energy estimates from profiling wind LiDAR measurements and their potential for wind energy applications

Valerie-M. Kumer [d, *], Joachim Reuder [d], Manfred Dorninger [a], Rudolf Zauner [c], Vanda Grubišić [a, b]

[a] Department of Meteorology and Geophysics, University of Vienna, Austria
[b] National Center for Atmospheric Research, Boulder, CO, USA
[c] VERBUND Hydro Power GmbH, Austria
[d] Geophysical Institute, University of Bergen, Bjerknes Center for Climate Research, Norway

ARTICLE INFO

Article history:
Received 30 November 2015
Received in revised form
19 May 2016
Accepted 10 July 2016

2010 MSC:
00-01
99-00

Keywords:
LiDAR
Turbulence
Wind turbine wakes

ABSTRACT

This study shows that turbulent kinetic energy (TKE) estimates, derived from static LiDARs in Doppler Beam Swing (DBS) mode, permit a qualitative and quantitative characterization and analysis of turbulent structures as wind turbine wakes, and convective or shear generated eddies in the lower atmospheric boundary layer. The analysed data, collected by a WINDCUBE™ v1 in a wind park in Austria, is compared to WINDCUBE™ v1 and sonic data from the WINd Turbine Wake EXperiment Wieringermeer (WINTWEX-W). Although turbulence measurements with a WINDCUBE™ v1 are limited to a specific length scale, processed measurements above this threshold are in a good agreement with sonic anemometer data. In contrast to the commonly used turbulence intensity, the calculation of TKE not only provides an appropriate measure of turbulence intensities but also gives an insight into its origin. The processed data show typical wake characteristics, as flow decelerations, turbulence enhancement and wake rotation. By comparing these turbulence characteristics to other turbulent structures in the atmospheric boundary layer, we found that convection driven eddies in the surface layer have similar turbulence characteristics as turbine wakes, which makes convective weather situations relevant for wind turbine fatigue considerations.

1. Introduction

The complex interplay between wind turbines and the atmospheric boundary layer is one of the key issues in understanding and predicting the performance of wind farms. One of the main parameters to be considered in this context is the turbulence that approaches a wind turbine. The turbulence characteristics, driven by atmospheric stability and wind shear, strongly depend on site, season and synoptic situation. The turbulence generated by mesoscale atmospheric processes, e.g. fronts, or by microscale phenomena, e.g. convection and local wind shear, not only affects the power generation but also structural parameters like peak loads and fatigue. This directly impacts the first row turbines as well as indirectly the whole wind farm, because the structure and dynamics of wind turbine wakes also change with the atmospheric conditions. Choosing the appropriate turbulence class is therefore a crucial site assessment decision for the overall park performance.

The definition of these turbulence classes is however mainly based on turbulence intensity (TI), a parameter defined as the standard deviation based on one-second measurements of the horizontal wind speed divided by its 10-min mean. Morales [1] already pointed out that there is much more information in two-point and higher-order statistics that should not be neglected. Consequently, we want to promote a different approach of investigating turbulence in the vicinity of a turbine by the turbulent kinetic energy (TKE), a parameter based on the variances of the wind components u, v, and w, an approach widely used in atmospheric boundary layer research [2]. Similar to TI, TKE can be derived from measurements of the three-dimensional wind vector and it can be related to the total available kinetic energy of the flow field. In contrast to TI, it also includes the vertical velocity component that can reach considerable values in particular in convection cells, over local surface inhomogeneities or in turbine wakes. The

* Corresponding author.
E-mail address: valerie.kumer@uib.no (V.-M. Kumer).

http://dx.doi.org/10.1016/j.renene.2016.07.014

TKE tendency equation can in addition be used to provide information on the origin of turbulence by an investigation of the relevant source and sink terms, which vary with the actual weather conditions [2].

Interactions between wind turbine performance and the atmospheric boundary layer have been studied quite intensively with Computational Fluid Dynamic models (CFDs) (e.g. Refs. [3–6]), wind tunnel experiments (e.g. Refs. [7–9]) and recently with LiDAR observations (e.g. Refs. [10–12]). While most of these recent LiDAR studies focus on wake measurements based on scanning Doppler LiDARs, we propose the qualitative and quantitative value of simple profiling Doppler Beam Swing (DBS) data to describe the turbulence characteristics of the atmospheric boundary layer (ABL) under the aspect of wind energy applications, including the investigation of wakes.

The estimation of turbulence parameters derived from DBS measurements is an active and partially controversial field of research that has indicated certain limitations [12,13]. Those are mainly related to the inherent general differences between an in-situ point measurement by cup or sonic anemometers and a volume-averaged value derived from LiDAR data, as well as from the wind vector reconstruction from subsequent line-of-sight measurements. Frehlich [14] shows that in the case of the WinTracer the measurement error due to volume averaging can be decreased by more flexible velocity estimation statistics that depend on local turbulence conditions. In terms of inaccuracies related to wind vector reconstructions from line-of-sight measurements Towers and Jones [15] show improvements for two-beam nacelle LiDARs with dynamic wind modelling and state estimation. For four-beam measurements the wind reconstruction is more accurate, but based on the assumption of homogeneous flow during one measurement circle, leading to lower sampling rates. In terms of e.g. wind speed variances, four-beam DBS measurements have a limitation in measuring small turbulent length scales compared to e.g. sonic measurements. This limitation is based on the lower DBS sampling rate of 1 Hz compared to sonic anemometer measurements taken at 10–100 Hz. DBS measurements can therefore not deliver turbulence information over the whole spectrum of boundary layer turbulence.

In this study, we aim to show that a qualitative and quantitative analysis of turbulence parameters obtained from simple DBS measurements, under consideration of those limitations, is reasonable. Consequently, we will present and analyse TKE estimates calculated from DBS LiDAR data of two LiDAR measurement campaigns for the characterization of turbulence at frequencies lower than the LiDAR sampling rate. We aim in this study to further investigate the potential and limitations of LiDAR based wind profile measurements for the characterization of the turbulence structure of wind turbine wakes under different meteorological conditions. The methods and results offer also an opportunity to the wind energy community to re-evaluate similar existing data sets that have not yet been investigated in detail under these aspects before.

The paper is organized as follows. Section two provides a description of the two measurement campaigns and the TKE retrieval used. Those TKE estimates are presented and analysed for three case studies for different meteorological conditions in Section three, providing valuable information relevant for peak loads and fatigue of wind turbines. Finally Section four presents a short summary and outlook.

2. Data and methods

2.1. Measurement campaigns

The study is mainly based on a data set collected by VERBUND Renewable Power GmbH. The measurement campaign took place at their wind park near Bruck an der Leitha in Lower Austria, over a three-month period, from 7 July through 6 October 2010. VERBUND deployed a WINDCUBE™ v1 165 m west of an Enercon 1.8 MW wind turbine with a hub height of 65 m and rotor diameter of 70 m (WEA4 in Fig. 1). This distance is equivalent to 2.5 rotor diameters (D), placing the WINDCUBE™ inside the wake area for easterly wind conditions. The site is characterised by agricultural fields, separated by small hatches and descends slightly towards South. In this study we use the raw DBS data collected by the WINDCUBE™ v1 (WLS7-85) from 25 August to 6 October 2010.

The WINDCUBE™ WLS7-85 measured radial wind speeds with a cone angle of 28° and a sampling rate of 1 s at nine measurement heights of 40, 65, 70, 85, 100, 135, 160, 185 and 200 m. The accuracy of the radial velocities is given as 0.2 ms^{-1} by the manufacturer [16] as long as the Carrier to Noise Ratio (CNR) is higher than −23 dB. The CNR depends on the atmospheric conditions and the aerosol content in the atmosphere [17]. During heavier rain or in the presence of low clouds the CNR drops below a software defined CNR threshold and calculations of the wind components, speed and direction are not carried out. The frequency of these data gaps defines the total data availability, which varied between 98% at lower measurement altitudes (<100 m) and 78% at 200 m during the campaign.

For validation of our turbulence estimates we include data from the WINd Turbine Wake EXperiment Wieringermeer (WINTWEX-W), conducted by the University of Bergen, Christian Michelsen Research AS and the Energy Research Centre of the Netherlands (ECN), as activity of the NORwegian Center for Offshore Wind Energy (NORCOWE) [18]. WINTWEX-W took place at ECN's wind turbine test site Wieringermeer [19] from November 2013 until mid of May 2014. Several Doppler LiDAR instruments were placed around and on top of the 2.5 MW NORDEX research turbine number 6 with a hub height and rotor diameter of 80 m. The site is characterised by agricultural land 4 m below sea level close to the coast line of the Wieringermeer. In this study we use raw data collected by the WINDCUBE™ v1 WLS7-67 and a Gill 3D sonic anemometer at 108 m height on the top of the collocated meteorological mast. The WLS7-67 was placed 3.25 D to the South-West of the turbine number 6, while the mast is situated in a distance of 2.5 D (Fig. 3). Similar to the WLS7-85, the WLS7-67 was set up in Doppler Beam Swing (DBS) mode with ten measurement heights of 40, 52, 60, 80, 100, 108, 120, 140, 160 and 200 m.

2.2. Calculation of turbulence parameters

Turbulence can either be studied by stochastic methods [1], or using a dynamic approach by applying governing momentum equations to a turbulent flow [2]. The former can be addressed by defining turbulence as the standard deviation σ_{vh} of a horizontal wind speed time series. This standard deviation can be normalized by the mean horizontal wind speed $\overline{v_h}$, resulting in the dimensionless parameter of *TI*

$$TI = \frac{\sigma_{v_h}}{\overline{v_h}}. \quad (1)$$

Another possibility to describe turbulence is to look at the energy of turbulent eddies, by splitting the total kinetic energy e into a mean ($\overline{e}$) and a perturbation part (e')

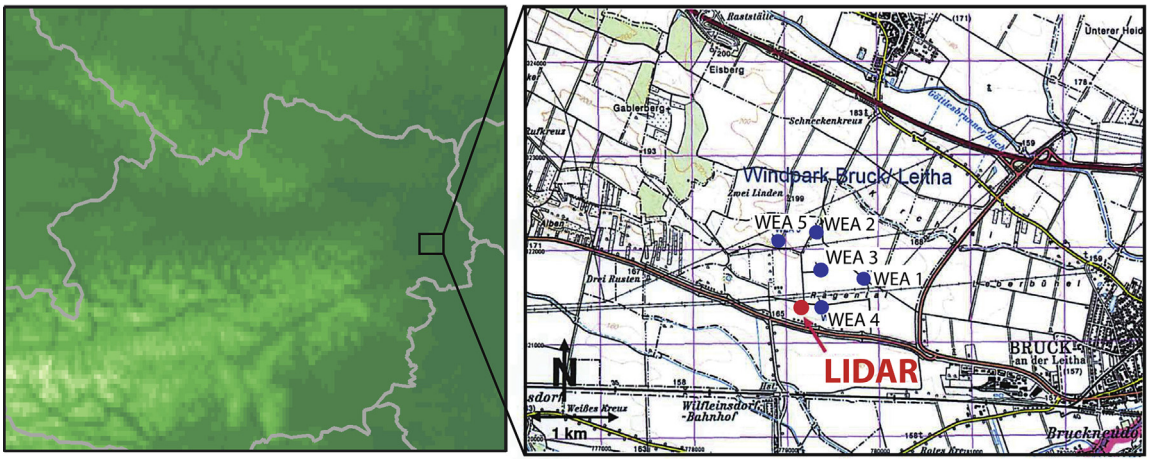

Fig. 1. Map of the wind park near Bruck an der Leitha and its location within Austria. The location of the WINDCUBE WLS7-85 is indicated with a red dot, the wind turbines WEA1 – WEA5 with blue dots. (For interpretation of the references to colour in this figure legend, the reader is referred to the web version of this article.)

$$e = \frac{1}{2}\left(u_k^2 + v_k^2 + w_k^2\right), \overline{e} = \frac{1}{2}\left(\overline{u}^2 + \overline{v}^2 + \overline{w}^2\right), e' = \frac{1}{2}\left(u_k'^2 + v_k'^2 + w_k'^2\right), \tag{2}$$

where u, v and w denote the three dimensional wind components. There is also a contribution to the total kinetic energy from the mean-turbulent products, but that part is an assumed to be very small and disappears after averaging. When averaging over a time window e' becomes more representative for the overall flow and can be written as a sum of the velocity variances and is referred to as *TKE*

$$TKE = \overline{e'} = \frac{1}{2}\left(\overline{u_k'^2} + \overline{v_k'^2} + \overline{w_k'^2}\right) = \frac{1}{2}\left(\sigma_u^2 + \sigma_v^2 + \sigma_w^2\right). \tag{3}$$

By applying the governing momentum equations to a turbulent flow it is possible to calculate the tendency of TKE [20]. Equation (4) represents a summary of the TKE tendency equation,

$$\frac{d\overrightarrow{e}}{dt} = T + AD = B + S + TT + P + D \tag{4}$$

which provides information on the origin of TKE. The term on the left-hand-side in Equation (4) is the total rate of change of TKE, which can be split into the local tendency *T* and advection *AD*. The total rate of change of TKE is generally non zero, reflecting the imbalance of the terms on the right-hand-side of Equation (4), which are buoyancy generation or consumption *B*, shear generation *S*, turbulent transport *TT*, pressure correlation *P* and dissipation *D*. Thus, TKE is not a conserved physical quantity and depends on different physical processes that can lead to generation and consumption of TKE.

In this study we could not fully calculate the TKE budget, mainly due to the lack of temperature, humidity and pressure measurements. Due to the wind vector retrieval technique, horizontal gradients of the wind field cannot be obtained from WINDCUBE™ v1 data. However, contributions to the TKE budget by vertical advection and vertical shear generation, as well as the tendency of TKE can be estimated by calculating forward differences in space and time respectively. From now on *AD* and *S* will always refer not to the total but to the vertical portion of advection and shear generation, respectively.

$$AD = -\overline{w}\frac{\partial\overline{e'}}{\partial z}, S = -\overline{u'w'}\frac{\partial\overline{u}}{\partial z} - \overline{v'w'}\frac{\partial\overline{v}}{\partial z} - \overline{w'w'}\frac{\partial\overline{w}}{\partial z}, T = \frac{\partial\overline{e'}}{\partial t} \tag{5}$$

In order to apply Equation (3) to our data set the wind data need to be transformed into the traditional meteorological coordinate system as Leosphere is using a different reference frame (Fig. 2). Additionally, Leosphere uses the last four cardinal direction measurements to project the radial wind speeds. As Sathe and Mann [13] showed, this technique can lead to an overestimation of turbulence as an eddy of a certain size can be measured twice. In order to avoid this potential interference, our estimates are based only on data from every 4th measurement, to assure that the time series consists of independent wind vectors, which is highlighted in Equation (6).

$$\begin{aligned}
&\overrightarrow{u}(k=1) = \overrightarrow{u}(vr_1, vr_2, vr_3, vr_4)\\
&\overrightarrow{u}(k=2) = \overrightarrow{u}(vr_2, vr_3, vr_4, vr_5)\\
&\overrightarrow{u}(k=3) = \overrightarrow{u}(vr_3, vr_4, vr_5, vr_6)\\
&\overrightarrow{u}(k=4) = \overrightarrow{u}(vr_4, vr_5, vr_6, vr_7)\\
&\overrightarrow{u}(k=5) = \overrightarrow{u}(vr_5, vr_6, vr_7, vr_8)\\
&\overrightarrow{u}(k=6) = \ldots
\end{aligned} \tag{6}$$

It should be noted that TKE retrieved from DBS data is only an estimation of TKE used in meteorology since the LiDAR measurement principle assumes homogeneous conditions during four beam measurements and cannot capture fluctuations smaller than the sampling rate. Therefore DBS data can only capture eddies that last longer than four seconds.

Since the original sampling rate of the WINDCUBE™ v1 is not constant over time, we interpolated the data on a regular time grid of $\Delta t = 4\ s$ for our spectral energy density calculations. Therefore, the time t can be represented as a whole-number multiple of Δt ($t = k^*\Delta t$). Following Stull [2], the coordinate frame was aligned into the main wind direction and the spectral energy density *S* was calculated by using the discrete Fourier transform *F* as follows:

$$S(f \neq f_n) = \frac{2*\left|F(f)\right|^2}{\Delta f} \quad \text{and} \tag{7}$$

$$S(f = f_n) = \frac{\left|F(f)\right|^2}{\Delta f} \quad \text{with} \tag{8}$$

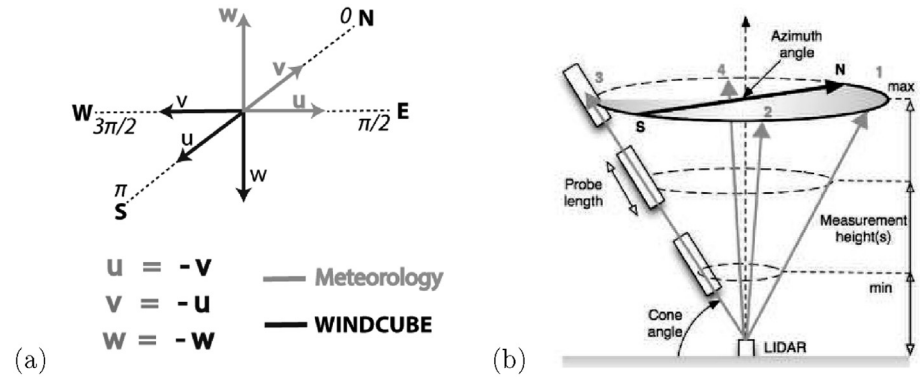

Fig. 2. (a) Definition of the two different coordinate systems, with the meteorological coordinate frame in grey and the one of the WINDCUBE™ in black. (b) Sketch of the measurement principle of the WINDCUBE™ [25].

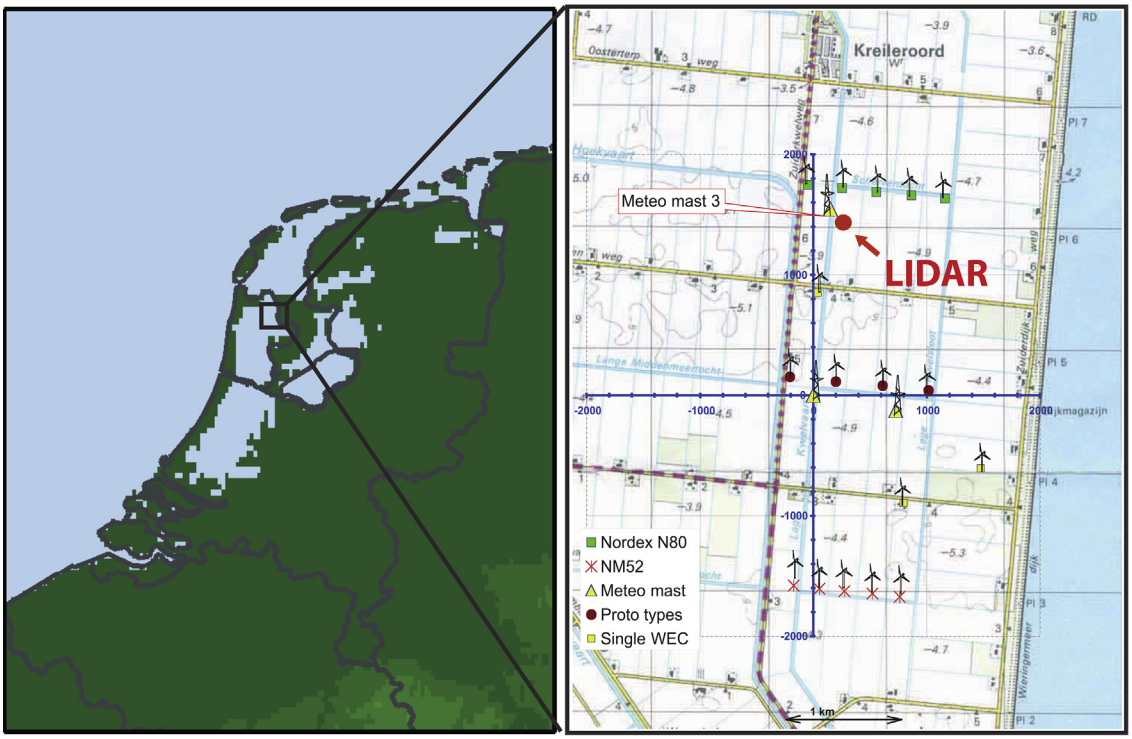

Fig. 3. Map of the Netherlands (left) and the wind turbine test site Wieringermeer (right). The locations of the WINDCUBE™ WLS67 is indicated with a red dot. (For interpretation of the references to colour in this figure legend, the reader is referred to the web version of this article.)

$$F(f) = \frac{1}{N}\sum_{k=0}^{N-1}(k\Delta t) * e^{2\pi f k \Delta t}. \tag{9}$$

The number of samples N equals to 3600 for $\Delta f = 0.25$ Hz, LiDAR data and 460800 for $\Delta f = 32$ Hz, sonic data.

For a validation of our TKE estimates against high frequency sonic measurements, we calculated the spectral energy densities S_{us} and $S_{e'}$ of the stream-wise wind component u_s, and the raw TKE estimate e', for two four-hour periods. It is important to keep in mind that these two four-hour periods are characterised by different turbulence conditions. In the first period the WINDCUBE™ v1 in Austria and the WINDCUBE™ v1 in the Netherlands face free-stream conditions (Fig. 4) while the devices in the second time series are located in the wake of their collocated wind turbines (Fig. 5). Important to keep in mind is that, the compared time series and spectra origin from measurements at different locations and different dates, and have been selected based on periods of similar and comparable mean wind conditions.

Figs. 4 and 5 present the time series for the chosen four-hour intervals in the top panel and the energy spectra S_{us} (left) and $S_{e'}$ (right) below, both averaged with a 180s window size. The black lines indicate the data from the sonic anemometer measurements at Wieringermeer, the blue lines the LiDAR data from the same site and the purple lines the LiDAR data from Bruck an der Leitha. To highlight the effect of different data processing methods, Figs. 4 and 5 show additionally to the spectra based on the four-second raw data, spectra of the one-second raw data (light grey) and for the four-beam-averaged data (dark grey) of the WLS7-67 at Wieringermeer.

The spectral curves retrieved from the one-second wind data of the WINDCUBE™ v1 follow the sonic measurements very closely

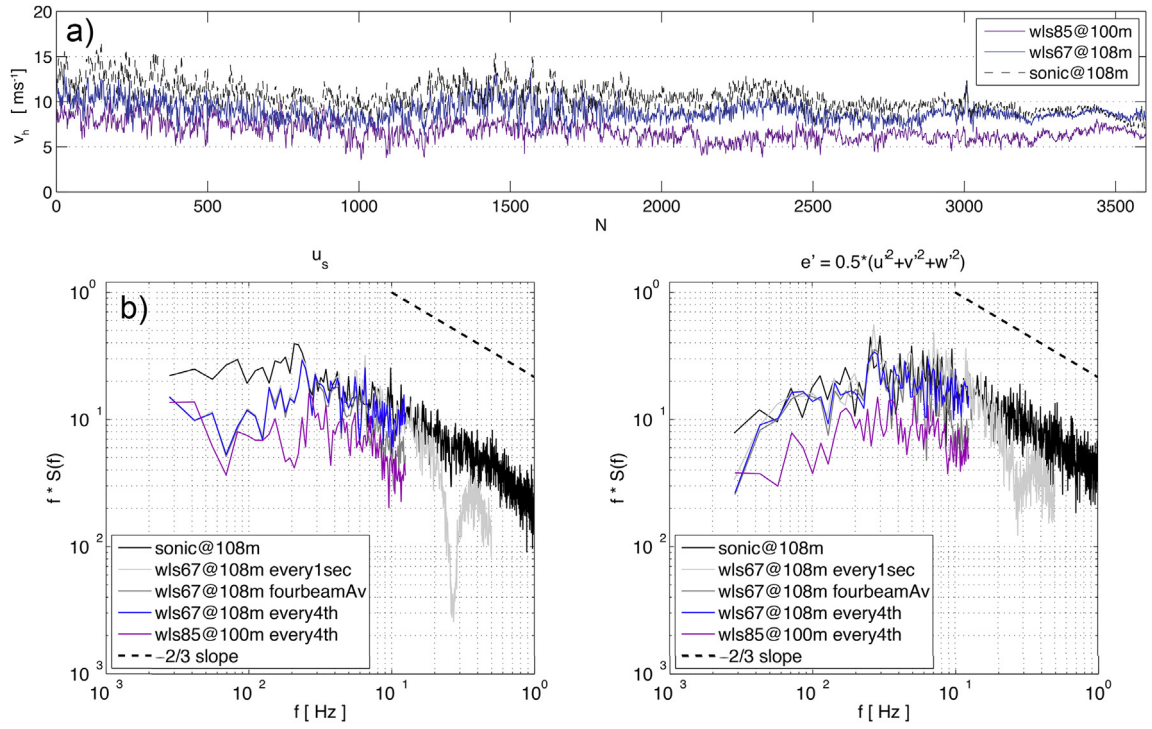

Fig. 4. (a) Time series of horizontal wind speed measurements of a sonic (black), the WLS7-67 (blue) from 15:00 to 19:00 CET on March 7th, 2014 and the WLS7-85 (purple) from 19:00 to 23:00 CET on August 26th, 2010. (b) Spectral plot of u_s and e' from sonic (black), one-second WLS7-67 (light grey), four beam average WLS7-67 (dark grey), four-second WLS7-67 (blue) and four-second WLS7-85 (purple) data. The black dashed line represents the theoretical −2/3 slope of a Kolmogorov inertial sub-range. (For interpretation of the references to colour in this figure legend, the reader is referred to the web version of this article.)

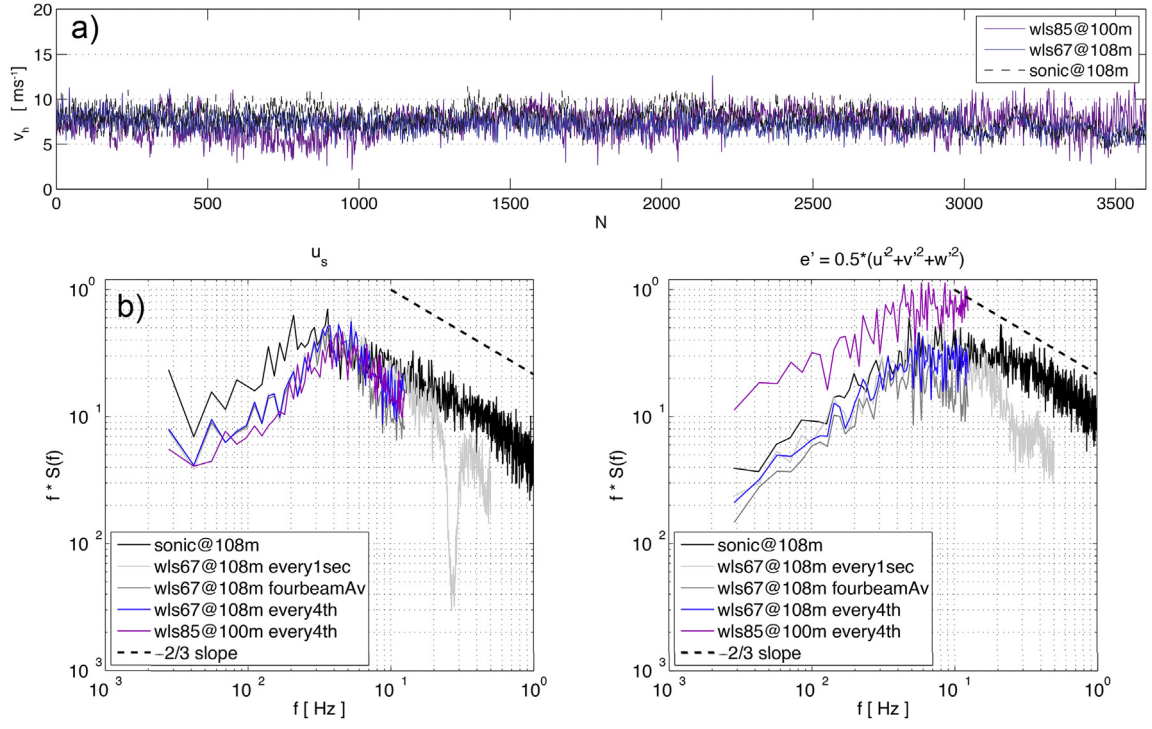

Fig. 5. (a) Time series of horizontal wind speed measurements of a sonic (black), the WLS7-67 (blue) from 00:00 to 04:00 CET on March 1th, 2014 and the WLS7-85 (purple) from 04:00 to 08:00 CET on September 25th, 2010. (b) Spectral plot of u_s and e' from sonic (black), one-second WLS7-67 (light grey), four beam average WLS7-67 (dark grey), four-second WLS7-67 (blue) and four-second WLS7-85 (purple) data. The black dashed line represents the theoretical −2/3 slope of a Kolmogorov inertial sub-range. (For interpretation of the references to colour in this figure legend, the reader is referred to the web version of this article.)

up to a frequency of around 0.15 Hz (Figs. 4 and 5). For higher frequencies, spectral attenuation occurs and the energy level falls below the level of the sonic measurements. As already pointed out by Canadillas [21], the high frequency end of the one-second spectrum is affected by the temporal averaging algorithm, programmed for the wind vector retrieval. This effect disappears in the four-second and beam-averaged data. The beam-averaged data has the same temporal resolution as the four-second data, as it represents an average of the one-second raw data after every completed measurement circle. However, the beam-averaging leads to an underestimation of the spectral energy densities of u_s and e' for frequencies higher than 6×10^{-2} Hz. Since the beam-averaging fails to correctly represents turbulent processes at higher frequencies, filtering for independent wind vectors is clearly the best pre-processing method for our purposes.

Focusing on the four-second spectra of both sites, they show interesting similarities. In the first case of free-stream condition, the mean horizontal wind speed and its standard deviation of around 9 ms^{-1} and 1.1 ms^{-1} in the Netherlands are compared to 7 ms^{-1} and 1.1 ms^{-1} in Austria. Although the absolute wind speed was slightly lower in Austria the standard deviation at both sites were identical. Lower wind speeds in Austria lead also to a lower spectral energy density of u_s and e' compared to the Netherlands. Apart from the magnitude of the spectra, the shape is the same for both locations. The spectra show a typical energy decay, which is at higher frequencies parallel to the slope of the Kolmogorov inertial sub-range. Despite the disagreement in the energy of u_s at the low-frequencies, the spectra agree well to the ones of the sonic measurements. The presence of upstream prototype turbines and a small mountain ridge may have an influence on the spectra from the WLS7-67, the sonic anemometer, and WLS7-85 respectively.

During the second case of wake conditions, both sites show identical values of 7 ms^{-1} mean horizontal wind speed and similar TI values of around 0.14 in the Netherlands and 0.16 in Austria. Only at the end of the period the variance is higher in Austria compared to the Netherlands. The spectral energy distribution of u_s peaks consistently at a frequency of around 3×10^{-2} Hz (Fig. 5). The source of the peak could potentially be related to wake meandering [22], but needs further investigations. For frequencies higher than the peak frequency the spectra is parallel to the slope of the Kolmogorov inertial sub-range. The low-frequency differences in the stream-wise wind component can be related to a slightly higher average horizontal wind speed in the sonic data. It is important to remember that the v1 and the sonic do not measure the exact same volume of air and that the v1 in the Netherlands measured at a different site and location relative to the wind turbine. The WLS7-85, as well as the sonic, collected data at 2.5 D, while the WLS7-67 measured at 3.25 D. Despite the different location, the spectral energy density of the raw TKE estimate from the WLS7-85 is of the same shape but at a higher overall level, which can mainly be explained by higher variability in the last hour of the selected time interval in Austria compared to the decreased variability in the Netherlands. A shorter time period of three hours would make the wind conditions more similar and might bring the energy level of TKE closer together. In addition, the closer location to the turbine, as well as the different turbine type and control systems may also have an effect.

Although the spectra of u_s from LiDAR and sonic measurements at Wieringermeer differ at low frequencies in both cases, the raw TKE estimate e' out of the four-second data is in good agreement with the raw TKE calculated from the 32 Hz sonic data. Also the limitation of not identical wind conditions at the different sites does not alter the similarities in spectral shape. These similarities give confidence that four-second LiDAR data can be beneficially used for further investigations based on the atmospheric TKE content.

3. Results

3.1. TI and TKE

The LiDAR wind measurements show a signal of channelled flow (Fig. 6a) at the Bruck an der Leitha site during the investigated period from 25 August to 6 October 2010. The terrain strongly favours north-westerly and south-easterly wind directions. The mean wind speed during the campaign was 5 ms^{-1} at 65 m altitude and the corresponding frequency distribution of the wind speeds is shown in Fig. 6b for four different heights. Most dominant wind speeds are not constant over height but shift towards higher speeds with increasing height. The maximum occurrence is not only shifted but also broadened. At 200 m the distribution gets bimodal, with a secondary maximum at around 11 ms^{-1}, potentially indicating the occurrence of low-level jets in the area. For the further investigations only wind speeds above the cut in wind speed of the turbines, i.e. 3 ms^{-1}, were taken into account.

Fig. 7 presents TI and TKE at five selected levels of 40, 65, 100,

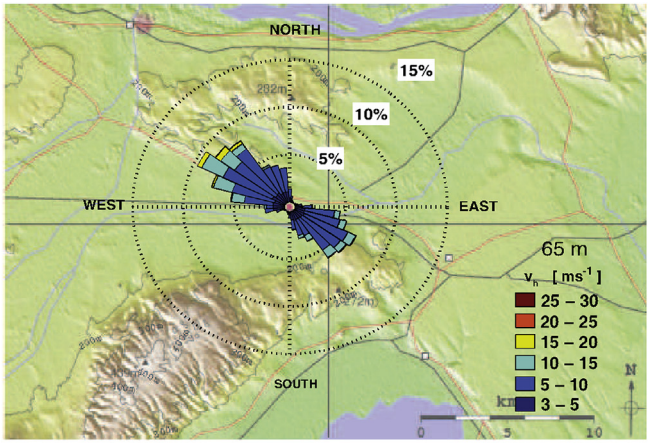

(a)

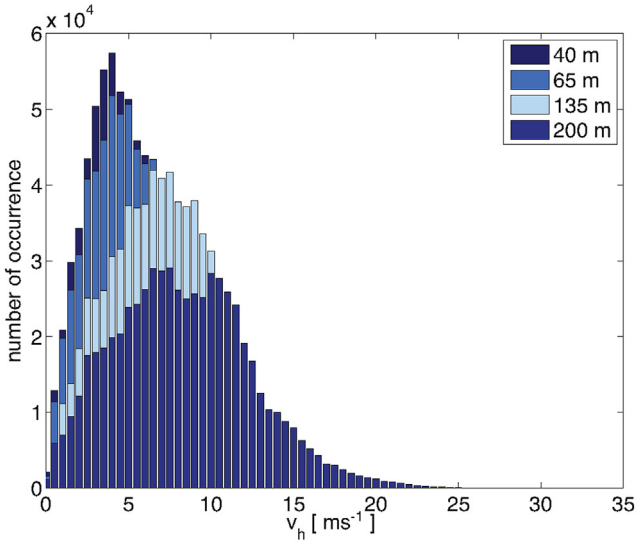

(b)

Fig. 6. a) Wind rose for wind speeds greater than 3 ms^{-1} at 65 m on top of the local topography. b) Horizontal wind speed frequency distributions at 40, 65, 135 and 200 m.

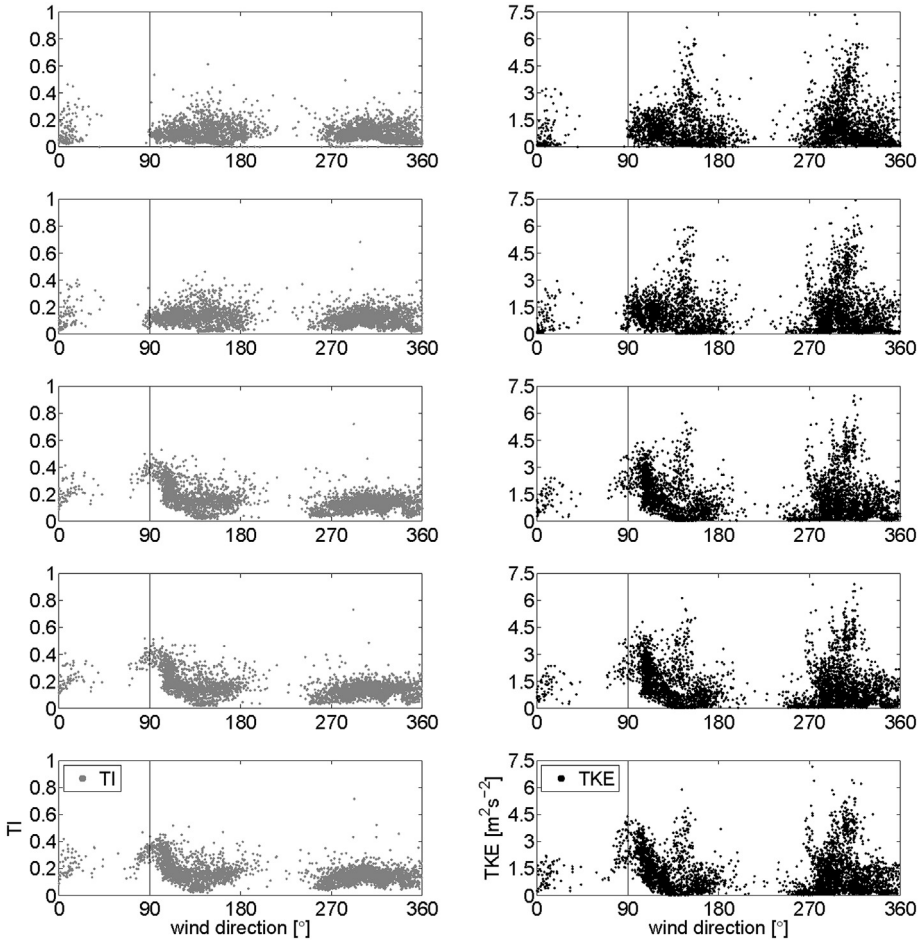

Fig. 7. TI (left) and TKE (right) calculated for wind speeds greater than 3 ms^{-1} for the whole analysed period as function of wind direction at 40, 65, 100, 135 and 200 m (from bottom until top). The vertical black line indicates the influence of the turbine wake for easterly winds.

135, and 200 m derived from the processed WINDCUBE™ LiDAR measurements, as function of the wind direction. It can be clearly seen that the distribution of turbulence is not constant over the directions and that the two turbulence measures contain different information. TI shows rather uniformly values below 0.2 throughout all measurement levels, except for easterly winds at around 90°, where the TI is distinctly enhanced. The corresponding peak value reaches approximately 0.4 for 40, 65, and 80 m (not shown) and 0.3 for 100 m, at higher levels it is completely absent. The plots for TKE show much more structure with values typically below 3 $m^2\ s^{-2}$ for most wind directions. Wind direction bands of higher TKE are associated with higher absolute wind speeds and can be found around 150 and 330°, clearly exceeding 5 $m^2\ s^{-2}$. Similar to TI, TKE also shows enhanced absolute turbulence values in the lower levels for the easterly directions. This signature of increased turbulence, which vanishes at altitudes above the blade tip height of 100 m, can be associated with the wake of the wind turbine WEA 4, located 2.5 D upstream of the WINDCUBE™ for this wind direction.

TI typically decreases for stronger winds, as it is normalized by the average wind speed. It gives therefore only a relative measure of the state of turbulence without any information with respect to e.g. peak loads on wind turbines and turbine blades. The overall TKE content of the flow is without doubt the more appropriate parameter for this purpose. The following plots will also show that the ratio between turbulent and mean kinetic energy, i.e. TKE/KE, defines a parameter with nearly the identical information content as TI. As a consequence TKE/KE can beneficially replace TI in case of the availability of 3D wind measurements, e.g. by 3D sonic anemometers or wind LiDARs.

For a better comparison of TI and TKE/KE, both parameters have been bin averaged over 15° intervals and are presented in the left column of Fig. 8. They show in general a nearly identical wind direction dependency, but also a distinct difference in the absolute values. The average values for TKE/KE are below 0.1 for all levels in no-wake conditions and increase to around 0.2 for the turbine wake in easterly flow. While the general level of TKE/KE is more or less independent of height, TI generally decreases with increasing altitude and wind speed. For the lower levels the undisturbed average values of TI are around 0.15 and decrease to approximately 0.1 for 200 m. In the easterly wind situation the average TI exceeds 0.3 at the lower, wake effected levels. For a closer look the corresponding scatter plots between TI and TKE/KE are presented in the right column of Fig. 8, where the color code separates between different wind speed intervals. The scatter of the data points generally decreases with increasing wind speed and with decreasing altitude, resulting in the highest correlation of both parameters for wind speeds above 15 ms^{-1} (indicated by the blue dots) close to the ground. It is also evident that the higher wind speed measurements are concentrated at the lower edge of the

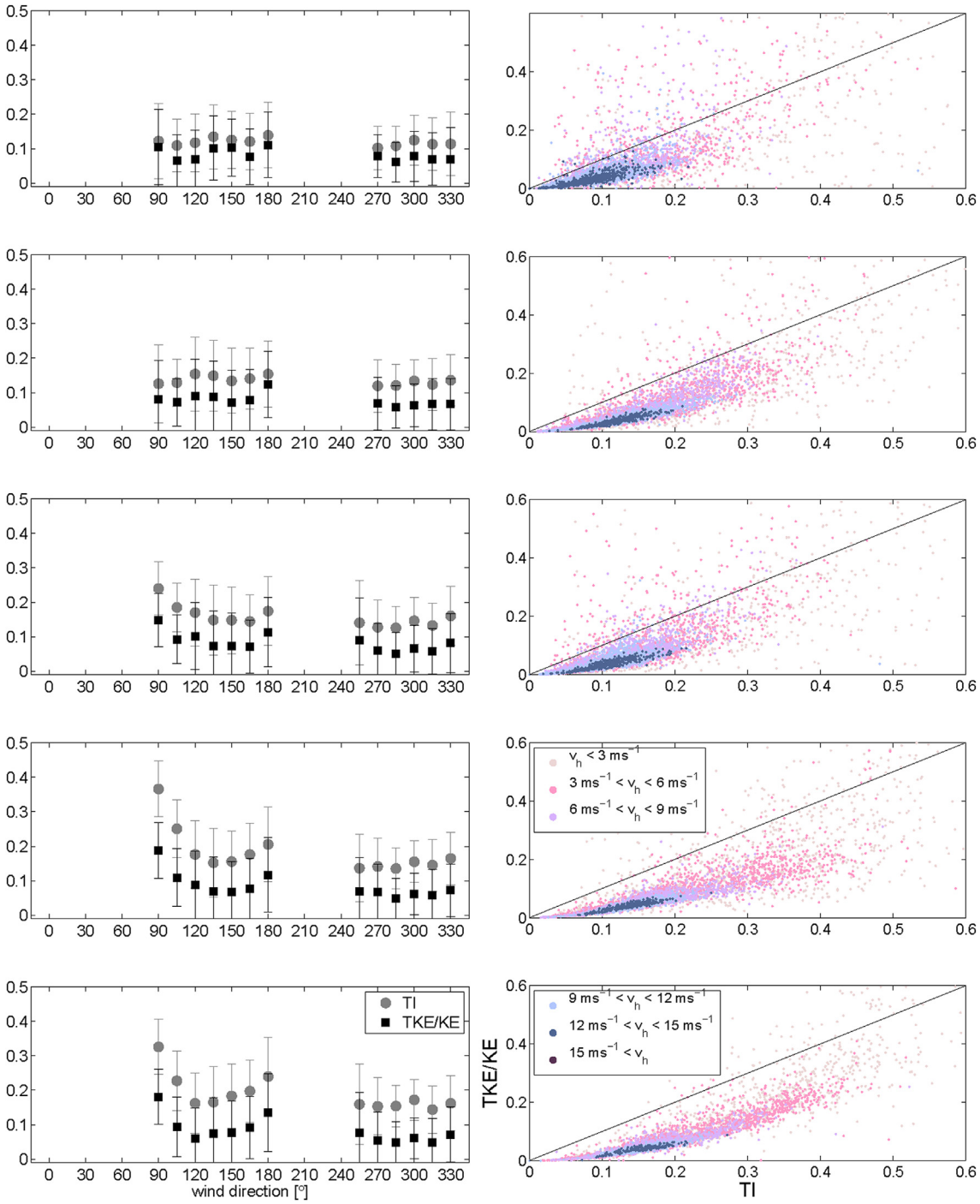

Fig. 8. TI (grey) and TKE/KE (black) binned over 15° wind direction intervals (left) and scatter plots of TI against TKE/KE binned and color-coded for 3 ms^{-1} wind speed intervals (right). The selected altitudes are from bottom to top 40, 65, 100, 135 and 200 m.

corresponding cloud of data points. The relationship between TI and TKE/KE seems to be nearly linear, except for the 40 m level that indicates a slightly parabolic curvature.

3.2. Case studies

Motivated by the results on the different information content of TKE and TI we will in the following present and analyse three selected case studies for wind energy relevant flow structures under different atmospheric conditions. This will include the detailed study of a complex wake affected situation, as well as undisturbed flow conditions in a neutral and a convective unstable boundary layer.

3.2.1. Complex flow

During the passage of a low pressure system east of Lower Austria on 25 September 2010, easterly winds dominated for several hours, leaving the WINDCUBE™ inside the wake of WEA4.

The wake region downstream of a wind turbine conceptually consists of a conical helix, expanding with increased distance

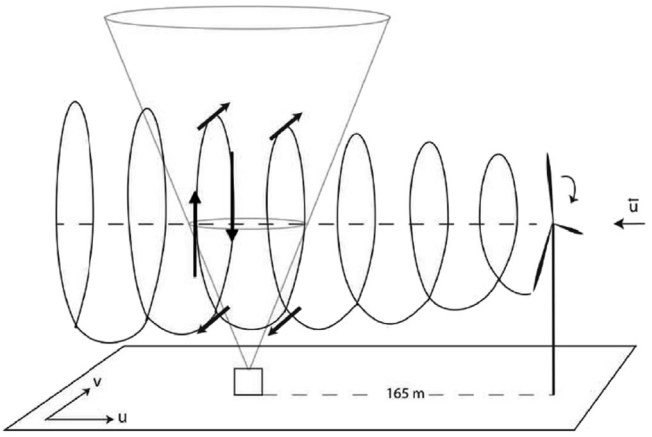

Fig. 9. Illustration of the LiDAR location inside the wake region during the easterly flow situation described. The arrows indicate the up- and downdraft couplet as well as the flow reversal in the meridional wind component.

downwind [23], as sketched in Fig. 9. Wind tunnel experiments by Zhang [4], showing an up- and downdraft couplet in a cross-section perpendicular to the rotation axis downwind of a turbine, support this picture.

The selection of contour plots from the measurements between 00:00 and 12:00 CET on 25 September 2010, presented in Fig. 10, clearly shows that the processed DBS data of the WINDCUBE™ v1 can capture basic wake characteristics, such as the deceleration of horizontal wind speed, the increased TKE, and the wake rotation. As the wind direction turned to 90°, the strong upwind part of the helix moved into the measurement range of the WINDCUBE™, with maximum vertical wind speeds of 1.1 ms^{-1} around hub height. In terms of its vertical extension, the helix elongates above 120 m, which is visible in the flow reversal of the meridional wind component at 110 m. The observed flow decelerations of 5 ms^{-1} compare well to measurements from a scanning LidAR by Iungo [24] reporting corresponding values of 4–6 ms^{-1}.

In order to understand turbulence generation inside the wake region, Fig. 11 presents profiles of vertical shear generation, vertical advection and TKE tendency, horizontal wind speed and TKE itself. To contrast the wake effects, two different times of the day are illustrated, one before the LiDAR was located inside the wake region (00:00 CET) and one during the wake event (08:00 CET). A strong shear line, induced by a wind turbine related deceleration of the horizontal wind speed from 13 ms^{-1} to 5 ms^{-1}, indicates that there is a large amount of turbulence generated by vertical wind shear. This vertical shear represents in this situation a major source of TKE with its maximum around blade tip height. Similar effects, e.g. strong shear below a low-level jet, appear on the top of a stable boundary layer during night-time conditions [2]. In both situations the vertical shear production of TKE would be the dominant source, with a tendency to generate anisotropic turbulence in this regions. The vertical shear generation for our case has a minimum around hub height and increases again below. The wake rotation seems also to trigger a weak but measurable vertical transport, reflected by the vertical advection of TKE. The vertical profiles of the TKE budget terms show in general that there is a non-uniform production of TKE with different local maxima. This leads to a complex turbulent wind pattern that propagates downstream. Affected downstream turbines face not only lower wind speeds and higher turbulence, but also fluctuations in the cross-stream wind component due to the wake rotation, that disturbs the lift of the rotor blades.

3.2.2. *Neutral flow*

To compare the previous results of complex flow conditions to a situation with the highest TKE estimates during the campaign, we analysed a strong wind case on September 1st, 2010. Triggered by a convergence zone of a high pressure system over the North Sea and a low pressure system over the Ukraine, north-westerly winds of around 15 ms^{-1} persisted during the whole day (Fig. 12). In this wind speed regime the boundary layer is well mixed and can be expected to be neutral. The wind speed profile has a classical

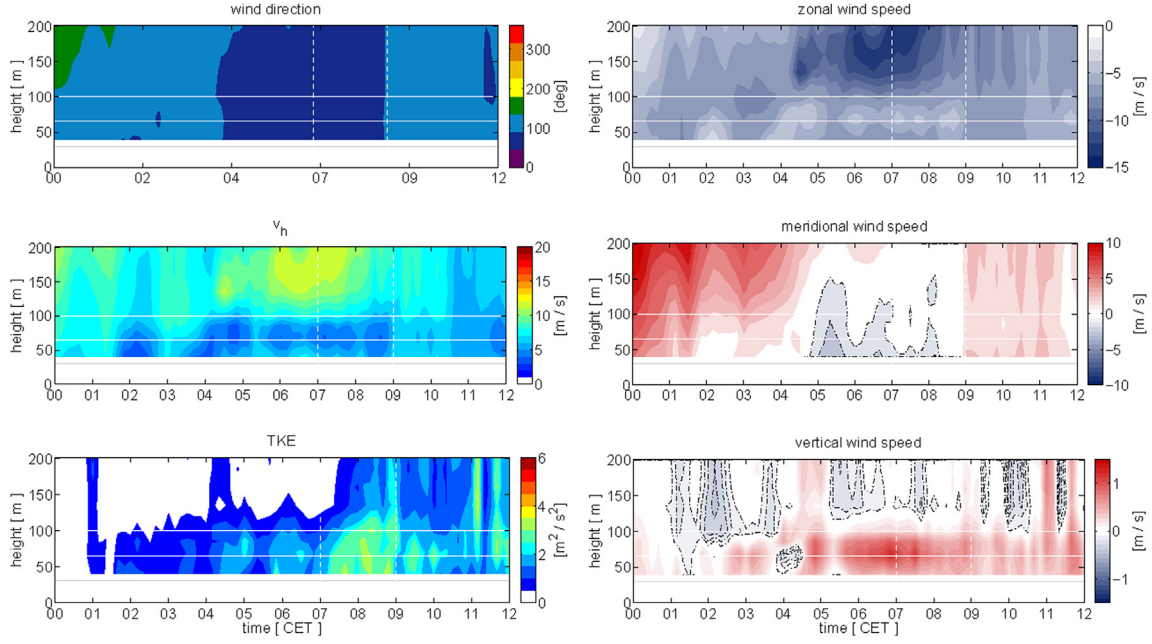

Fig. 10. Contour plots of wind direction, horizontal wind speed and TKE (left) and the three wind components (right) on 25 September 2010 using 10 min block averages of the processed raw data. The horizontal white and grey lines at 100 m, 65 m and 30 m indicate blade tip, hub and blade bottom height of the wind turbine. The dashed vertical lines marks the time frame during which the TKE profiles were calculated. Dashed contours correspond to negative values.

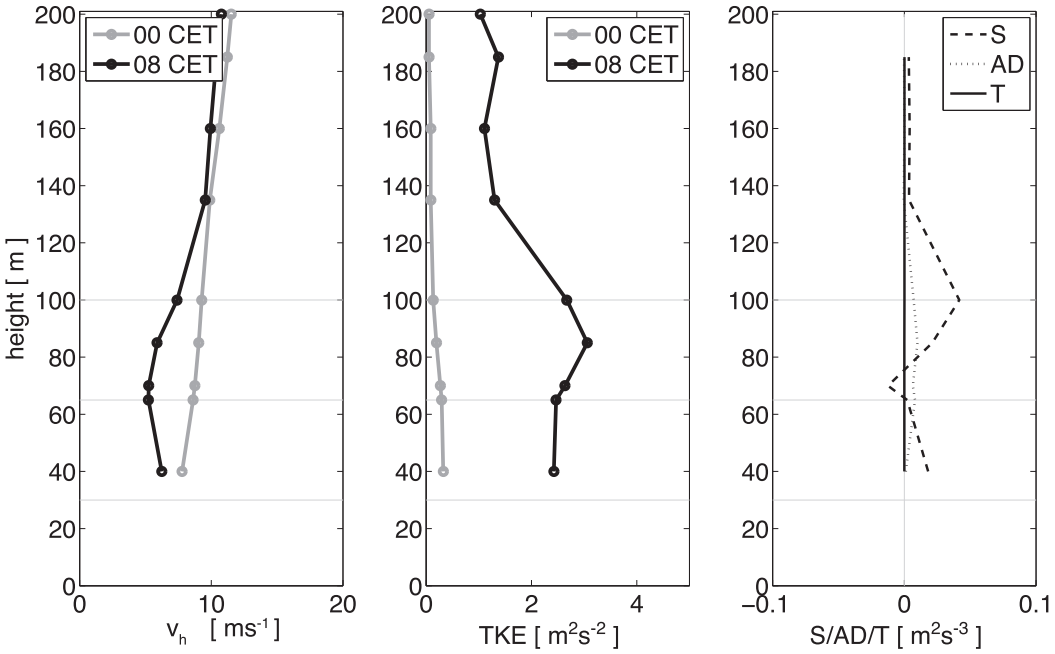

Fig. 11. Profiles of horizontal wind speed (left), TKE (center) and TKE budget terms (right) at 00:00 CET and 08:00 CET on 25 September 2010. S, AD and T are calculated as two-hour averages between 07:00 to 09:00 CET and represent vertical shear generation, vertical advection and TKE tendency, respectively. Markers indicate data points, while horizontal lines represent the levels of blade tip, blade bottom and hub height.

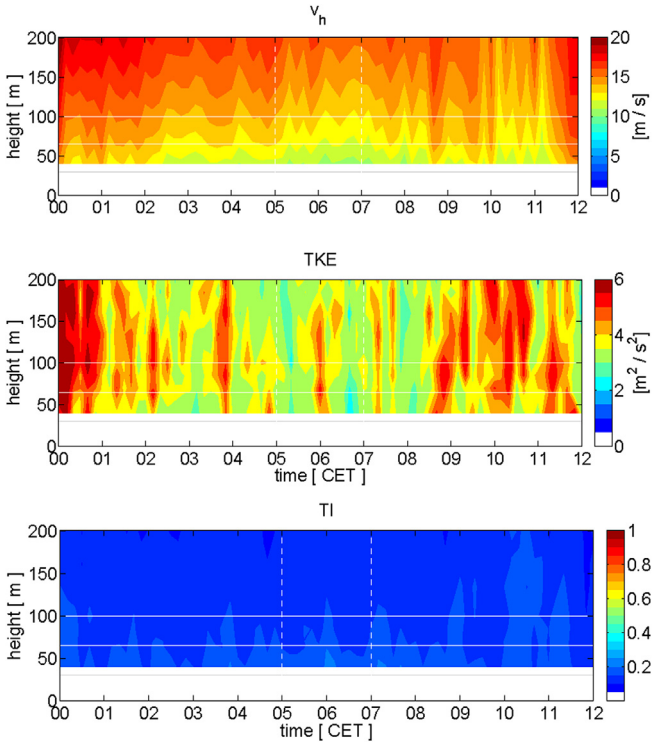

Fig. 12. Contour plots of horizontal wind speed, TKE and TI on September 1st, 2010 using 10 min block averages of the processed raw data. The horizontal white and grey lines at 100 m, 65 m and 30 m indicate the levels of blade tip, hub and blade bottom height of the wind turbine. The dashed vertical lines marks the time frame during which the TKE profiles were calculated.

logarithmic shape (left panel in Fig. 13). As TKE is proportional to the wind speed, this case represents one of the TKE maxima of the whole analysed period (Fig. 7), with TKE reaching values of 6 m^2 s^{-2}. The absolute turbulence level is in general very high throughout the day with some local maxima in TKE, which might be related to gusts. Compared to TKE, TI shows a much more homogeneous picture with highest values of 0.2 at lowest measurement altitudes.

The high winds come along with strong vertical wind speed gradients, leading to shear generation of TKE at all measurement heights. In general the vertical shear generation is increasing towards the ground, indicating the influence of surface roughness effects. The vertical advection term is of minor importance and basically limited to the level close to the nacelle height.

3.2.3. *Unstable flow*

Another natural source of turbulence is convection. Therefore, this case describes turbulence characteristics of a convectively unstable flow occurring on 5 September 2010. Synoptic forcing was weak during that day and northerly winds with rather low wind speeds of about 5 ms^{-1} prevailed. Triggered by a still strong enough radiative forcing a convective boundary layer (CBL) could establish during the day. This is documented by the evolution of TKE from 04:00 to 15:00 CET (Fig. 14). With sunrise, the boundary layer develops from stable night-time to unstable day-time conditions. Vertical wind speed gradients disappear and the ABL turns into a layer of almost constant horizontal wind speed with height. In contrast to the earlier discussed cases, the turbulence is buoyancy driven by vertical heat fluxes, leading to an average TKE level of around 2 m^2 s^{-2}. TI varies between 0.1 and 0.2 with similar but less distinct characteristics as TKE during the day. The vertical shear generation and advection are negligible and considerably smaller than for the other two cases (Fig. 15). Under these conditions of instability and enhanced vertical motion, turbulent eddies will again be anisotropic with a large vertical extension, which might lead to additional, so far not accounted for, fatigue of turbines.

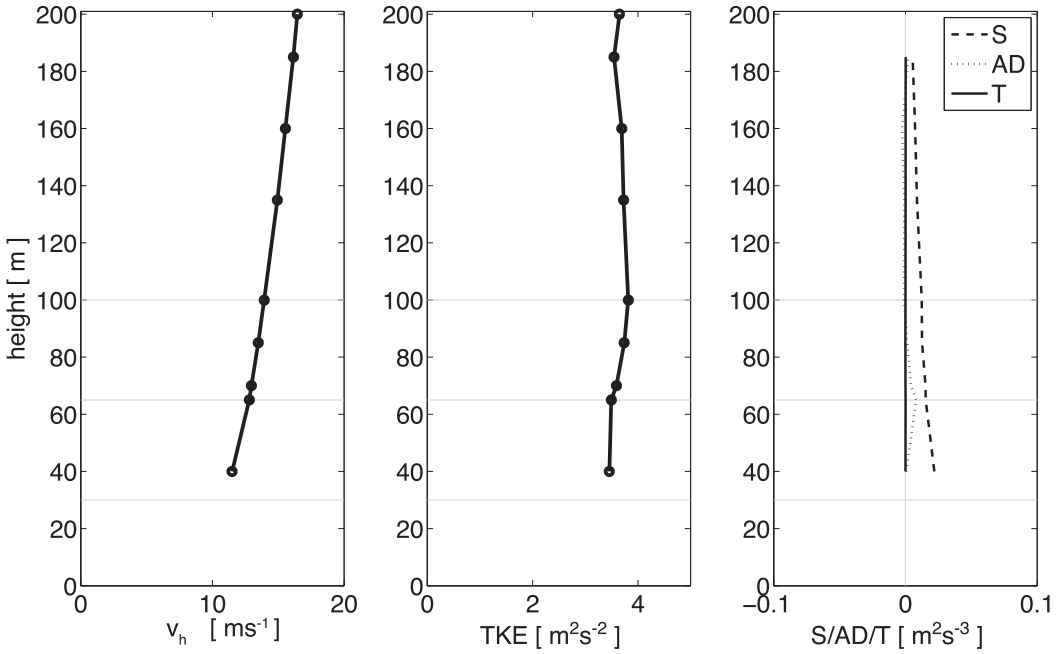

Fig. 13. Profiles of horizontal wind speed (left), TKE (center) and TKE budget terms (right) averaged between 05:00 and 07:00 CET on 1 September 2010. S, AD and T stand for vertical shear generation, vertical advection and TKE tendency, respectively. Markers indicate data points, while horizontal lines represent the levels of blade tip, blade bottom and hub height.

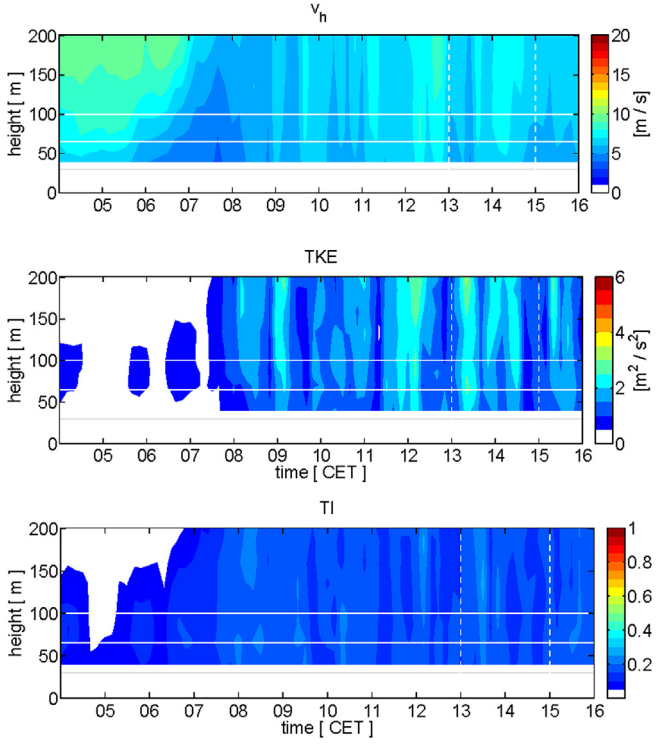

Fig. 14. Contour plots of horizontal wind speed, TKE and TI on September 5th, 2010 using 10 min block averages of the processed raw data. The horizontal white and grey lines at 100 m, 65 m and 30 m indicate blade tip, hub and blade bottom height of the wind turbine. The dashed vertical lines marks the time frame during which the TKE profiles were calculated.

3.3. Discussion

Fig. 16 summarizes the results of the three case studies presented above. It shows, from left to right, the profiles of TI, TKE and TKE/KE averaged over two hours representative for the discussed situations. The profiles represent the neutral case from 05:00 to 07:00 CET on September 1st in blue, the unstable case from 13:00 to 15:00 CET on September 5th in orange, and the wake case from 07:00 to 09:00 CET on September 25th in black. Symbols highlight corresponding maximum and minimum values during the selected two hour periods. All three panels illustrate the influence of wake effects at altitudes below 135 m, especially in comparison with the more or less height constant profiles during the two other cases. TI displays a distinct local maximum around nacelle height, while TKE/KE and also TKE slightly, but monotonously increase towards the ground.

A more detailed comparison of the neutral and convective cases, shows only small differences in TI, with nearly identical values at 40 m. However, there is a clear decrease of TI with altitude for neutral conditions while the TI for the convective situation is constant with height. The decrease in TI in case of increasing wind speeds with height indicates again the effect of normalising the standard deviation by the absolute mean wind speed. In contrast to TI, the normalisation of TKE by KE shows in both situations a nearly identical but altitude constant profile with a distinct difference in the absolute level. Although the level of turbulence is 2% higher, compared to the neutral case, the absolute TKE values are much smaller. The convective case, with relatively weak horizontal winds, has average TKE values of 1.5 $m^2\ s^{-2}$ and maximum values of around 5 $m^2\ s^{-2}$. In the neutral case, with strong horizontal winds, the corresponding values are 3.5 $m^2\ s^{-2}$ and 9 $m^2\ s^{-2}$.

Compared to the wake case, the undisturbed neutral case has distinctly higher absolute TKE values, both in average and maximum. Looking at the observed maximum values of TKE/KE, the profiles also indicate that a rather low wind convective situation can reach TKE/KE levels close to those inside of a turbine wake, a

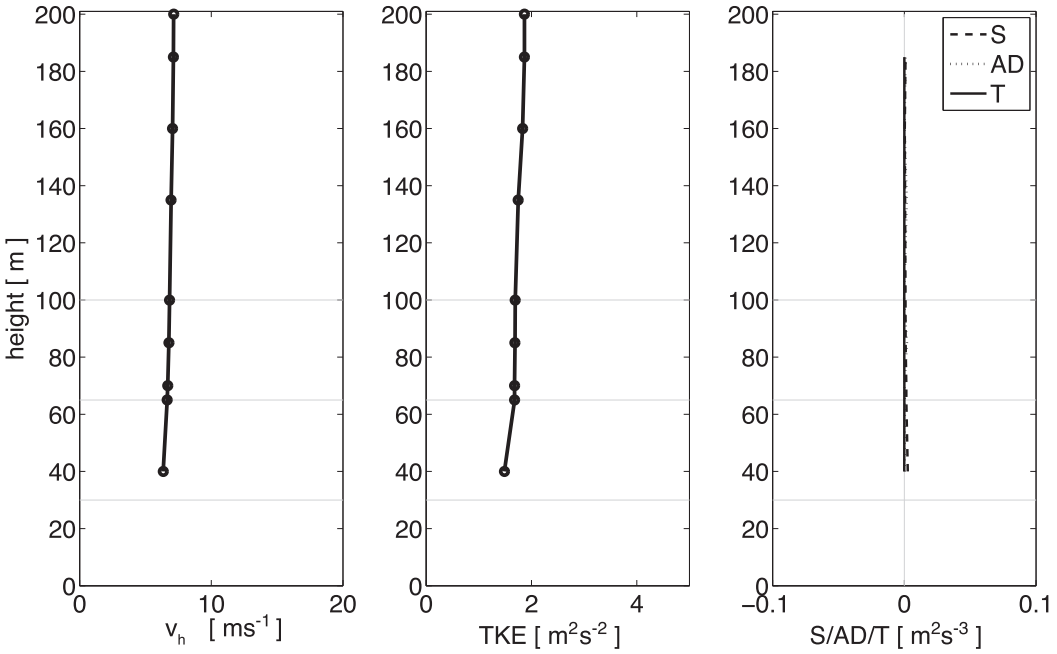

Fig. 15. Profiles of horizontal wind speed (left), TKE (center) and TKE budget terms (right) averaged between 13:00 and 15:00 CET on 1 September 2010. S, AD and T represent vertical shear generation, vertical advection and TKE tendency, respectively. Markers indicate data points, while horizontal lines indicate blade tip, blade bottom and hub height.

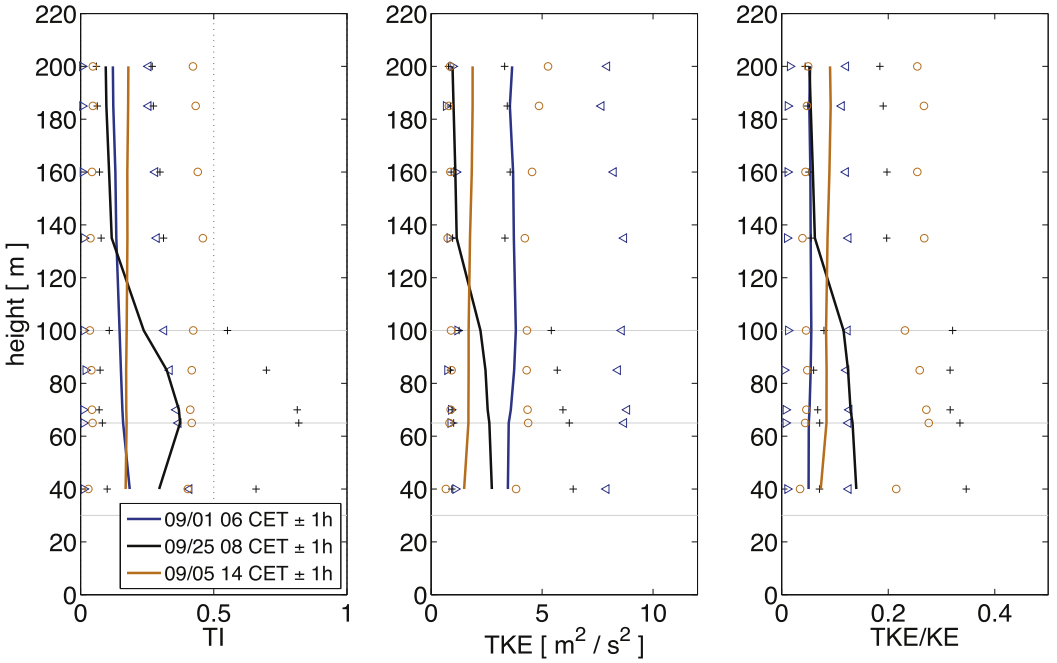

Fig. 16. Two hour averaged profiles of TI (left), TKE (middle) and TKE/KE (right) for the three investigated case studies, a neutral ABL in rather strong wind conditions on September 1st, 2010 (blue lines), a convective ABL on 5th September 2010 (orange line) and a wake case on September 25th, 2010 (black lines). The symbols indicate the minimum and maximum values observed during the corresponding two-hour period. The horizontal lines mark the levels of blade tip, blade bottom and hub height. (For interpretation of the references to colour in this figure legend, the reader is referred to the web version of this article.)

fact that could be of importance under the aspect of long-term fatigue. The presented comparison among the three case studies shows the importance of the consideration of different turbulence characteristics and parameters for the appropriate understanding and description of short-term peak loads as well as the long-term fatigue of wind turbines exposed to different atmospheric flow regimes.

4. Conclusion

This study presents an analysis of TKE estimates derived from Doppler LiDAR DBS raw data, collected with a WINDCUBE™ v1 during a measurement campaign in a wind park near Bruck an der Leitha in Lower Austria. By processing the one-second DBS data in terms of a wind vector transformation to the meteorological

coordinate system, a filter for independent wind vectors and a linear interpolation on a constant, four-second time grid, we retrieved a good TKE estimate with respect to sonic anemometer measurements.

The TKE estimates compare not only well to sonic data from the WINTWEX-W under free stream but also under wake conditions and deliver information similar to TI when normalised by the total kinetic energy of the flow. With additional information of generation terms, TKE has more to offer than the commonly used TI.

To illustrate the differences between TKE and TI we analysed the turbulence distribution of our main data set and compared three different case studies in terms of their turbulence characteristics. The turbulence distribution of TKE/KE and TI showed highest percentage of turbulence when the device was inside the wind turbine wake. However, highest absolute turbulence values related to strong north-westerly winds, clearly exceed the measured wake values. This information is not contained in the TI distribution, although it is valuable for peak load calculations.

Though our analysis is limited to the turbulence spectra captured with the given temporal resolution of the WINDCUBE™ v1, the study shows that processed DBS data can capture different turbulence characteristics and show significant differences between the three cases. Turbulence of a neutral ABL with high wind speeds seems to be only relevant for peak load calculations, as the level of turbulence in the mean flow is with 10% rather low. The turbulence distribution is rather homogeneous over the rotor disc with slightly increasing vertical shear generation towards the ground. For unstable conditions the buoyancy induced vertical mixing increases the percentage of turbulence almost to the levels observed inside a wake. Similar to the neutral case the turbulence is homogeneously distributed over the rotor disk.

In the contrasting case of a wake downstream of a wind turbine, the flow shows a strong shear region around blade tip height, resulting in an inhomogeneous flow propagating further downstream. Additionally to lower wind speeds and increased turbulence, fluctuations of the cross-stream component, induced by the wake rotation, might lead to disturbances in the lift of downstream turbines. As a consequence those wind turbines face unequally distributed loads, influencing not only the power production but also the lifetime by increased fatigue. For a more detailed study of the spatial variability of atmospheric turbulence in the future, the use of several distributed static wind LiDAR systems, potentially complemented by scanning LiDARs would be beneficial to increase the spatial coverage by horizontal (PPI) or vertical scan patterns (RHI), both of the ambient flow and in turbine wakes. For a consequent application of the proposed TKE budget approach to identify and quantify the sources of turbulence, collocated measurements of the temperature profile should be performed.

Finally we would like to emphasize that the methods and results presented in this study can be used to re-evaluate corresponding available observational data sets that have not yet been investigated under these aspects before. The authors are confident that this will be a rather cost-efficient way to increase our knowledge of the interaction of boundary layer flow and wind turbines.

Acknowledgements

The research presented was partially supported by the Theoretical Meteorology Group at the University of Vienna and the Norwegian Center for Offshore Wind Energy (NORCOWE) funded by the Research Council of Norway (RCN) under project number 193821. We thank our colleagues Stefano Serafin and Lukas Strauss from the University of Vienna who provided insight and expertise that greatly assisted the presented research. The WINTWEX-W campaign was using instrumentation of the OBLO (Offshore Boundary Layer Observatory) infrastructure project, also founded by RCN (project number 277770).

References

[1] A. Morales, M. Wächter, J. Peinke, Characterization of wind turbulence by higher-order statistics, Wind Energy 15 (3) (2012) 391–406, http://dx.doi.org/10.1002/we.478 arXiv:arXiv:1006.4405v1.
[2] R.B. Stull, An introduction to boundary layer meteorology, Book 13 (1988) 666, http://dx.doi.org/10.1007/978-94-009-3027-8.
[3] D. Mehta, A.H. van Zuijlen, B. Koren, J.G. Holierhoek, H. Bijl, Large eddy simulation of wind farm aerodynamics: a review, J. Wind Eng. Ind. Aerodyn. 133 (2014) 1–17, http://dx.doi.org/10.1016/j.jweia.2014.07.002.
[4] W. Zhang, C.D. Markfort, F. Porté-Agel, Near-wake flow structure downwind of a wind turbine in a turbulent boundary layer, Exp. Fluids 52 (5) (2011) 1219–1235, http://dx.doi.org/10.1007/s00348-011-1250-8.
[5] Y.-T. Wu, F. Porté-Agel, Simulation of turbulent flow inside and above wind farms: model validation and layout effects, Boundary Layer Meteorol. 146 (2) (2013) 181–205, http://dx.doi.org/10.1007/s10546-012-9757-y.
[6] B. Sanderse, S.P. Pijl, B. Koren, Review of computational fluid dynamics for wind turbine wake aerodynamics, Wind Energy 14 (7) (2011) 799–819, http://dx.doi.org/10.1002/we.458.
[7] L.P. Chamorro, F. Porté-Agel, Turbulent flow inside and above awind farm: a wind-tunnel study, Energies 4 (2011) 1916–1936, http://dx.doi.org/10.3390/en4111916.
[8] P.E. Hancock, F. Pascheke, Wind-tunnel simulation of the wake of a large wind turbine in a stable boundary layer: part 2, the wake flow, Boundary Layer Meteorol. 151 (1) (2014) 23–37, http://dx.doi.org/10.1007/s10546-013-9887-x.
[9] P.-Å. Krogstad, L. Sætran, M.S. Adaramola, “Blind Test 3” calculations of the performance and wake development behind two in-line and offset model wind turbines, J. Fluids Struct. (2014), http://dx.doi.org/10.1016/j.jfluidstructs.2014.10.002.
[10] M.E. Rhodes, J.K. Lundquist, The effect of wind-turbine wakes on summertime US midwest atmospheric wind profiles as observed with ground-based doppler lidar, Boundary Layer Meteorol. 149 (2013) 85–103, http://dx.doi.org/10.1007/s10546-013-9834-x.
[11] G. Iungo, F. Porté-Agel, Volumetric scans of wind turbine wakes performed with three simultaneous wind LiDARs under different atmospheric stability regimes, J. Phys. Conf. Ser. 524 (2014) 012164, http://dx.doi.org/10.1088/1742-6596/524/1/012164.
[12] J.K. Lundquist, M.J. Churchfield, S. Lee, A. Clifton, Quantifying error of lidar and sodar Doppler beam swinging measurements of wind turbine wakes using computational fluid dynamics, Atmos. Meas. Tech. 8 (2015) 907–920, http://dx.doi.org/10.5194/amt-8-907-2015.
[13] A. Sathe, J. Mann, J. Gottschall, M.S. Courtney, Can wind lidars measure turbulence? J. Atmos. Ocean. Technol. 28 (7) (2011) 853–868, http://dx.doi.org/10.1175/JTECH-D-10-05004.1.
[14] R. Frehlich, Upstream Measurements of Wind Profiles with Doppler Lidar for Improved Wind Energy Integration, Tech. Rep, Golden Field Office, Golden, CO (United States), oct 2012, http://dx.doi.org/10.2172/1053852.
[15] P. Towers, B. Ll Jones, C.B. Ll Jones, Real-time wind field reconstruction from LiDAR measurements using a dynamic wind model and state estimation, Wind Energy (2014), http://dx.doi.org/10.1002/we.1824.
[16] C. Aussibal, WINDCUBE User's Manual, 2008.
[17] M.L. Aitken, M.E. Rhodes, J.K. Lundquist, Performance of a wind-profiling lidar in the region of wind turbine rotor disks, J. Atmos. Ocean. Technol. 29 (3) (2012) 347–355, http://dx.doi.org/10.1175/JTECH-D-11-00033.1.
[18] V.-M. Kumer, J. Reuder, B. Svardal, C. Sætre, P. Eecen, Characterisation of Single Wind Turbine Wakes with Static and Scanning WINTWEX-W LiDAR Data, 80, 2015, http://dx.doi.org/10.1016/j.egypro.2015.11.428.
[19] J.G. Schepers, T.S. Obdam, J. Prospathopoulos, Analysis of wake measurements from the ECN wind turbine test site wieringermeer, EWTW, Wind Energy 15 (4) (2012) 575–591, http://dx.doi.org/10.1002/we.488.
[20] P. Markowski, Y. Richardson, Mesoscale Meteorol. Midlatitudes (2010), http://dx.doi.org/10.1002/9780470682104.
[21] B. Canadillas, A. Bégué, T. Neumann, Comparison of turbulence spectra derived from LiDAR and sonic measurements at the offshore platform FINO1, in: 10th German Wind Energy Conference (DEWEK 2010), No. Dewek, 2010, pp. 18–21.
[22] Y.-A. Muller, S. Aubrun, C. Masson, Determination of real-time predictors of the wind turbine wake meandering, Exp. Fluids 56 (3) (2015) 53, http://dx.doi.org/10.1007/s00348-015-1923-9.
[23] W. Tong, Wind Power Generation and Wind Turbine Design, 2010.
[24] G.V. Iungo, Y.-T. Wu, F. Porté-Agel, Field measurements of wind turbine wakes with lidars, J. Atmos. Ocean. Technol. 30 (2) (2013) 274–287, http://dx.doi.org/10.1175/JTECH-D-12-00051.1.
[25] A. Clifton, D. Elliott, M. Courtney, RECOMMENDED PRACTICES FOR REMOTE SENSING FOR WIND ENERGY APPLICATIONS, IEA wind.